

Combinatorial Discovery of Novel Amphiphilic Polymers for the Phase Transfer of Magnetic Nanoparticles

Benjamin W. Muir,^{*,†} Bradford A. Moffat,[‡] Peter Harbour,[†] Greg Coia,[†] Guoliang Zhen,[†] Lynne Waddington,[†] Judith Scoble,[†] Daniel Krah,[†] San H. Thang,[†] Yen K. Chong,[†] Paul Mulvaney,[§] and Patrick Hartley[†]

CSIRO Molecular and Health Technologies, Bayview Avenue, Clayton, 3168 Australia, Department of Radiology, The University of Melbourne, Parkville, 3050 Australia, and Department of Chemical Engineering, The University of Melbourne, Bio 21, Parkville, 3050 Australia

Received: May 25, 2009; Revised Manuscript Received: August 3, 2009

In this paper, we present a new approach to the combinatorial discovery of amphiphilic maleic anhydride copolymers which can be used as a generic method for the optimization and control of hydrophobic nanoparticle phase transfer into the aqueous phase. This combinatorial multiwell chemical screening process resulted in the discovery of ‘hit’ polymer ring opened chemistries that allow the spontaneous and highly efficient phase transfer of superparamagnetic iron oxide (SPIO) nanoparticles into water under ambient conditions. Effective polymer–SPIO materials were screened for magnetic properties via a high-throughput (HT) magnetic resonance imaging (MRI) technique and nanoparticles were successfully tested for stability in buffer. It was found that the water-soluble SPIO nanoparticles could be tuned somewhat in terms of their MRI relaxivities via the specific ring-opening molecules used. To impart effective charge and steric stability of the water-soluble nanoparticles in buffer, the molecular weight, and chemistry of any given maleic anhydride copolymer was critical. Particle sizing via dynamic light scattering and cryo-transmission electron microscopy analysis showed significant discrepancies in the mean particle sizes obtained. This HT approach and the new amphiphilic polymers discovered have potential for use in various nanotechnology applications.

Introduction

The use of metal inorganic nanoparticles is an area of significant research, and in the past decade the field of nanomaterials has grown rapidly.^{1–4} Nanoparticles are widely used in the materials sciences from solid-state devices to various biomedical applications.^{2,3} The most common use of nanoparticles in the ‘life sciences’ is research conducted into the development of diagnostic and therapeutic agents *in vitro*, and *in vivo*.^{4,5} Few inorganic nanoparticle formulations are yet to successfully make it through the clinic and into the marketplace.⁶ This highlights the immense physicochemical, biological, and regulatory hurdles that confront the nanotechnologist when it comes to devising successful nanoparticle and coating formulations.⁵ Of all the nanoparticle chemistries being studied for use *in vivo*, research into quantum dot and magnetic nanoparticles are by far the largest growing fields.^{4,5}

In the ‘life sciences’ superparamagnetic iron oxide nanoparticles (SPIOs) are of great interest^{7–11} and have been used in applications as varied as magnetic resonance imaging (MRI),^{5,12–17} drug delivery,¹⁸ magnetic separation, and treatment of hyperthermia. One of the greatest challenges to the materials scientist for the preparation of suitable inorganic nanoparticles is the production of stable, biocompatible surface chemistries that provide SPIO stabilization in water and, more specifically, buffered solutions. To date, the most commonly used coatings include poly(ethylene glycol)-¹⁹ and dextran⁶-based polymeric

coatings owing to their ‘stealth’-like properties *in vivo*, slowing down their uptake by the reticuloendothelial system (RES). When SPIOs are produced they can be made via organic or aqueous solvent production methods. It is commonly accepted that the organic solvent routes allow for the most control over nanoparticle size, shape, crystal structure, and other important properties.²⁰ The challenge with these preparation methods is that they generally result in the production of hydrophobic nanoparticles capped with organic lipid ligands which do not readily disperse in water. Therefore, there is a vast body of research dedicated to the investigation of new phase-transfer chemistries.²¹ Generally the approach is to stabilize the nanoparticles with polymers or small molecules that either bind through metal coordination of the iron oxide cores²² or through the interdigitation of hydrophobic groups between the nanoparticle and phase transfer compound (hydrophobic–hydrophobic interactions).²¹

The use of maleic anhydride copolymers for the water phase transfer of hydrophobic nanoparticles was first reported by Pellegrino et al.²³ The hydrophobic regions on the copolymer are used to interdigitate with the hydrophobic groups on the nanoparticle (commonly oleic acid) while the anhydride group is ring opened to produce water-soluble functionalities across the polymer backbone.²⁴ The reaction of a primary or secondary amine and other nucleophiles can result in the formation of a mixed amide-carboxylic acid system for example. In the preceding 4 years, only a handful of ring-opening molecules and maleic anhydride copolymers have been reported since the seminal paper by Pellegrino et al.^{23,25–33} This may perhaps in part be due to the difficulty of obtaining nanoparticles that are stable for prolonged periods in buffer. Some clinically used

* To whom correspondence should be addressed. E-mail: ben.muir@csiro.au.

[†] CSIRO Molecular and Health Technologies.

[‡] Department of Radiology, The University of Melbourne.

[§] Department of Chemical Engineering, The University of Melbourne.

SPIO agents such as Resovist^{6,34} are not stable in PBS for prolonged periods of time.

The aim of this study was to develop an efficient technology for the synthesis and characterization of phase transfer water-stabilized SPIOs. In previous work we have shown the effective use of a low-molecular-weight poly(styrene-maleic anhydride) copolymer for the effective phase transfer of quantum dot nanoparticles.³⁵ In this work, we introduce a high-throughput (HT) technique to screen for novel ring-opening polymer chemistries that allow the phase transfer of hydrophobic SPIO nanoparticles from the organic phase into the aqueous phase. This work greatly expands the number of known amphiphilic polymers that can be utilized to phase transfer organic nanoparticles into aqueous solutions. It was postulated that reaction of the anhydride group with various amines may allow the screening of various nanoparticle properties including solubility, relaxivity, size, and chemical functionality for subsequent reaction with biomolecules or cross-linking of the anhydride polymer chains around the iron oxide nanoparticle core. These ‘hit’ polymer–nanoparticle phase transfer SPIOs were then further analyzed for their MRI relaxation properties using a previously reported³⁶ HT MRI protocol. This technique allows for the quantification of MRI longitudinal relaxation rate constants (R_1), and transverse relaxation rate constants (R_2 and R_{2^*}) of multiple samples simultaneously in a clinical MRI scanner. The MRI contrast performance of SPIOs is characterized by their relaxivities which is the rate at which R_1 , R_2 , and R_{2^*} change with concentration.

Experimental Methods

SPIO Production. SPIO nanoparticles were produced by a modified method published first by Park et al.²⁰ Sodium hydroxide (4.8 g, 120 mmol) was dissolved in 50 mL of distilled water and 80 mL of ethanol was then added. Oleic acid (40 mL, 120 mmol) was slowly added to the mixture solution with stirring and adjusted to pH 7.0. Iron chloride ($\text{FeCl}_3 \cdot 6\text{H}_2\text{O}$, 10.8 g, 40 mmol) was dissolved in 10 mL of distilled water and added to the above mixture, and then 140 mL of hexane was added. The resulting solution was heated to 70 °C for 4 h. When the reaction was completed, the upper organic layer containing the iron–oleate complex was washed three times with 30 mL of distilled water in a separation funnel. After washing, hexane was evaporated off, resulting in the formation of a waxy solid. To produce monodisperse iron oxide nanoparticles with a particle size of 8 nm used in this work, 7.2 g (8 mmol) of the iron–oleate complex and 1.14 g of oleic acid (4 mmol, Aldrich, 90%) were dissolved in 40 g of 1-octadecene (Aldrich, 90%) at room temperature. The reaction mixture was first heated to 100 °C and degassed for 30 min, then heated to 320 °C in 50 min and kept at that temperature for 15 min. The resulting brown-black solution containing the nanoparticles was then cooled to room temperature. The iron oxide nanoparticles were precipitated out of 1-octadecene by acetone and then redispersed in chloroform. The above procedure was repeated six times to obtain pure iron oxide nanoparticles as a solid powder. As an internal control for MRI experiments, Resovist (Bayer Schering), a clinically used SPIO formulation, was used.

Polymer Production. A commercial poly(octadecene-*co*-maleic anhydride) (PMAO) (CAS no. 25266-02-8) with M_n 30–50k from Sigma-Aldrich was used in the primary screen to test for effective ring-opening chemistries. A second series of four polymers was made via the RAFT process were then produced and screened with the best ‘hit’ amine candidates from the primary screen. Solvents were of AR grade and were distilled

TABLE 1: Molecular Weight (M_n), Polydispersity Index (M_w/M_n), and Percent Monomer Conversion Data for the Maleic Anhydride Copolymers Used in This Work

copolymer	M_n	M_w/M_n	conv (%)
P1	6500	1.53	37.9
P2	2000	1.16	95.0
P3	6400	1.30	99.8
P4	4900	2.31	14.9
P5	30–50k	N/A	N/A

before use. Monomers, styrene (from Sigma-Aldrich, ≥99%) and *n*-butyl vinyl ether (from Fluka, ≥97%) were purified by filtration through alumina (to remove inhibitors), distilled, and flash distilled immediately prior to use. Maleic anhydride (from Fluka, ≥99%) was recrystallized twice from chloroform before use. 1-Octadecene was obtained from Fluka (≥95%) and used as received. Initiators, α,α' -azobisisobutyronitrile (AIBN) was obtained from Tokyo Kasei and recrystallized twice from chloroform–methanol; 2,2'-azobis(2,4,4-trimethylpentane) (VR110) was purchased from Wako and used as received. Gel permeation chromatography was performed on a Waters Associates liquid chromatograph equipped with differential refractometer and a set of Waters Ultrastryagel columns (10^6 , 10^5 , 10^4 , 10^3 , 500, and 100 Å). Tetrahydrofuran (1.0 mL/min) was used as eluent. Conversions were determined gravimetrically. NMR spectra were obtained with a Bruker AC200 spectrometer on samples dissolved in deuteriochloroform. Chemical shifts are reported in ppm from TMS. FTIR spectra were obtained with a Perkin-Elmer 2000 FT-IR spectrophotometer, in transmission mode using KBr as the background reference.

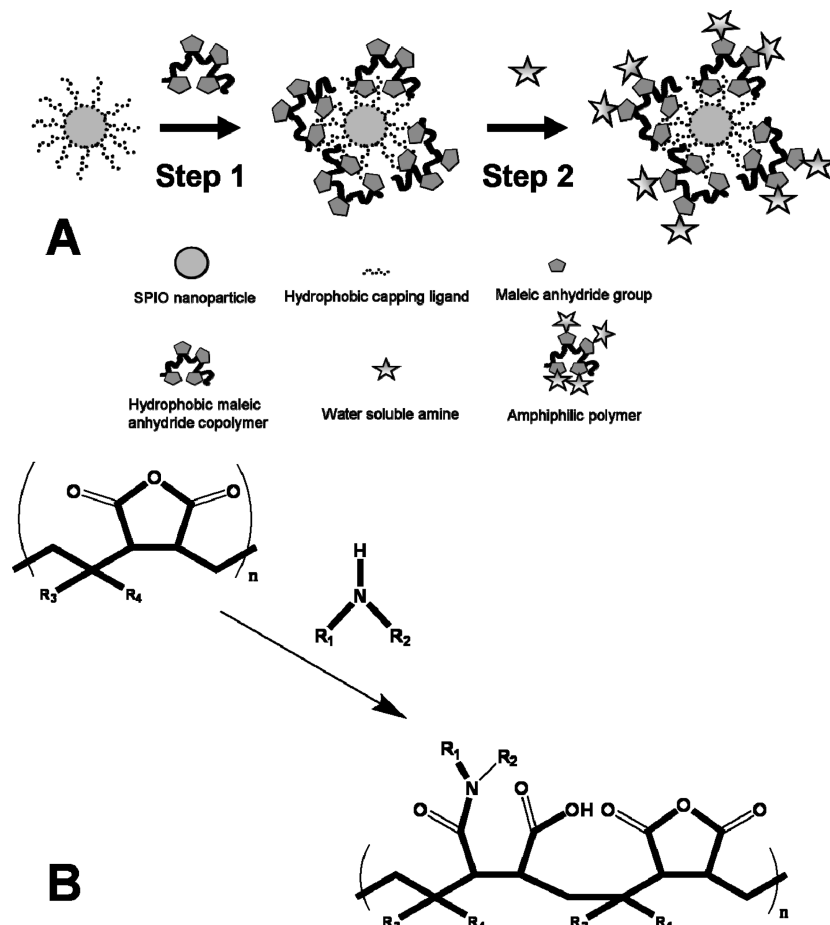
The RAFT agents *S*-cyanomethyl *S*-dodecyl trithiocarbonate³⁷ and 2-phenylpropan-2-yl dithiobenzoate³⁸ used were prepared as described previously. Described next is the procedure used to produce the 4 polymers used in this work with the RAFT agents described above.

Polymer P1: PMAO. An ampule containing 1-octadecene (4.51 g, 0.0179 mol), maleic anhydride (2.0 g, 0.0233 mol), *S*-cyanomethyl-*S*-dodecyl trithiocarbonate (95 mg, 2.99×10^{-4} mol), and VR110 (20 mg, 7.87×10^{-5} mol) was degassed by three repeated freeze–pump–thaw cycles ($\sim 10^{-3}$ mmHg) and then flame-sealed. It was allowed to polymerize at 100 °C for 64 h. The copolymer P1 (2.46 g, 37.9% yield) was isolated after removing unconverted 1-octadecene and maleic anhydride on Kugelrohr at 100 °C (0.005 mmHg). The GPC results of the copolymer P1 were M_n 6483; M_w/M_n = 1.53 and are summarized in Table 1. The copolymer was analyzed by ¹H NMR and FT-IR to confirm its purity and composition.

Polymers P2 and P3: Poly(styrene-*alt*-maleic anhydride). Copolymerizations of styrene and maleic anhydride (1.2:1 molar ratio) in the presence of 2-phenylpropan-2-yl dithiobenzoate in two concentrations were carried out. Two ampules were used, each contains styrene (2.5 mL, 0.0218 mol), maleic anhydride (1.78 g, 0.0181 mol), and RAFT agent 0.490 (1.80×10^{-3} mol) and 0.122 g (4.48×10^{-4} mol), respectively. The ampules were degassed by three freeze–pump–thaw cycles and flame-sealed. The ampules were heated at 110 °C for 16 h. Unconverted styrene was removed by evaporation and the residue was precipitated twice from ethyl acetate into *n*-hexane (to remove maleic anhydride) to give polymers P2 and P3, the results of which are summarized in Table 1.

Polymer P4: Poly(*n*-butyl vinyl ether-*co*-maleic anhydride). A stock solution of maleic anhydride (1.70 g, 0.017 mol), *n*-butyl vinyl ether (5.4 mL, 0.042 mol), and AIBN (19.4 mg, 1.18×10^{-4} mol) was slowly made to 10 mL mark (volumetric

SCHEME 1: (A) Schematic Representation of the Method Used to Screen for Novel Amphiphilic Copolymers^a (B) Generic Anhydride Ring-Opening Chemistry Used to Test for the Phase Transfer of Novel Hydrophobic Nanoparticles into Water via the Use of Maleic Anhydride Copolymers^b



^a In step 1, hydrophobic maleic anhydride copolymers are incubated with the hydrophobic nanoparticle surface. In step 2, hydrophilic amine-containing molecules are reacted with the MA units along the SPIO immobilized polymer backbone. If the polymer chemistry is successful, the resultant amphiphilic polymer will phase transfer the SPIO nanoparticle solution into water. ^b The reaction of a primary or secondary amine forms a mixed amide-carboxylic system where the hydrophobic group of the polymer interdigitates with the oleic acid capped nanoparticles. The anhydride component imparts water solubility to the SPIOS if the polymer and ring-opening chemistry are suitable.

flask) with isopropyl acetate. An aliquot (5 mL) of stock solution was placed in an ampule containing RAFT agent *S*-cyanomethyl-*S*-dodecyl trithiocarbonate (150 mg, 4.73×10^{-4} mol). The contents of the ampule were degassed by three repeated freeze-pump-thaw cycles, then flame-sealed, and heated at 60 °C for 16 h. The copolymer P4 (0.87 g, 14.9% conversion) obtained was purified by repeated precipitation four times (from ethyl acetate into *n*-hexane) to remove some unreacted maleic anhydride. The molecular weight and polydispersity data are summarized in Table 1.

Polymer P5: Poly(octadecene-*co*-maleic anhydride). This polymer was purchased from Sigma-Aldrich (CAS no. 25266-02-8), and has a M_n of 30–50k (polydispersity was not supplied).

HT Phase Transfer Screening. A HT screen was devised to test for novel ring-opening polymer chemistries for the phase transfer of hydrophobic SPIO nanoparticles. The reaction of a primary or secondary amine with the anhydride groups along the polymer backbone forms a mixed amide-carboxylic system (Scheme 1). The phase transfer is believed to occur via the interdigitation of the hydrophobic groups of the anhydride copolymer with the oleic acid capped nanoparticles. The ring-opened anhydride component subsequently imparts water solubility to the SPIO nanoparticles if the polymer and ring-opening

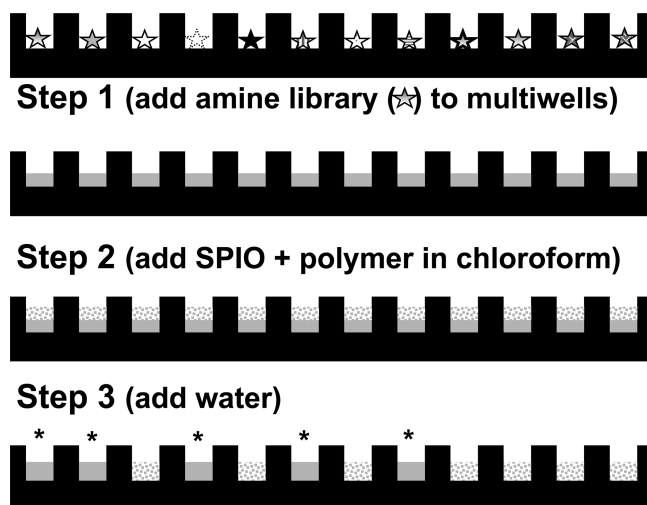
chemistry are suitable. If a particular compound was seen to phase transfer the nanoparticles after reaction with the maleic anhydride copolymer, it was termed a ‘hit’.

All 87 predominantly amine compounds whether solid or liquid were used as received from the manufacturer (Table 2). The polymer phase transfer reactions were carried out in 96-well polypropylene plates (Scheme 2). One drop, or one spatula ladle (~ 1 mg) of each amine compound, depending on whether the compound was a liquid or solid under ambient conditions was added to each well at 3-fold redundancy. Then 50 μ L of SPIO (1 mg/mL SPIO) solution containing 10 wt % of the polymer in chloroform was added to each well. To each well 150 μ L of Milli-Q water was then added and the plate was then heated with a heat gun to remove the chloroform. The reaction was considered to have worked if the resulting multiwell became dark brown after removal of the chloroform indicating suspension of the nanoparticles in water. To the wells with dispersed nanoparticles, 15 μ L of 10× PBS was then added and the solutions were left for 1 month. Only wells that still had suspended nanoparticles after this time (i.e., a dark brown solution) were classified as ‘hits’ and used for scale up and bulk testing. Scale up of the successful ring-opening chemistries was performed by adding 2 mL of SPIOs in chloroform and adding 6 mL of 1 M amine solution above the chloroform phase in a

TABLE 2: List of Amines Used to React with Maleic Anhydride Copolymers in Solution with SPIO Hydrophobic Nanoparticles in an Attempt to Make Them Water-Soluble

ethanolamine	2-amino hexanoic acid	1,4,8,11-tetraazacyclotetradecane-5,7-dione
1-acetyl piperazine	L-cysteine hydrochloride	1,4,8,11-tetraazacyclotetradecane
glycine anhydride	D,L-asparagine	tetraazacyclododecane tetrahydrochloride
mitomycin C	D,L-serine	bilirubin
ciprofloxacin	L-alanine	1,2-bis(3-aminopropylamino)ethane
O-benzyl-L-serine	L-valine	triethylenetetramine
nitrophenyl-N-acetyl-beta-D-galactosaminide, p-acetylneurameric acid, N-polyoxyethylenebis(amine)	N-methylhydroxylamine HCl	N-methyl-D-glucamine
	2-mercaptopropane sulfonic acid	diethyl-4-aminobenzylphosphonate
	4,5,6-triamino-2(1 <i>H</i>)-pyrimidinethione sulfate	5-nitouracil
kanamycin	dithiooxamide	
piperazine diacrylamide	2-mercaptopropionyl glycine	4,5-diamino-2-mercaptopurimidine
2-mercaptopropane hydrochloride	D,L-isoleucine	4,5-diamino-2,6-dimercaptopurimidine
cystamine	hydrazine sulfate	N-acetyl piperazine
L-cysteine-HCl	riboflavin	sarcosine
Jeffamine	amino-PEG-methoxy	2-(2-aminoethoxy)ethanol
N,5-dimethyl-3-phenylisoxazole-4-carboxamide	tris(2-aminoethyl)amine	morpholine
4-amino-5-imidazolecarboxamide hydrochloride	bis(2-hydroxyethyl)ethylenediamine	2-(methoxyethyl)amine
D,L-alanine	N,N-bis(hydroxyethyl)trimethylenediamine	4-amino-1-butanol
L-arginine	cytochrome C	n-butylethanolamine
L-alanine methyl ester HCl	diethyl formamidomalonate	2-(aminoethylamino) ethanol
4,6-diamino-2-mercaptopurimidine	Jeffamine-1000	N,N-bis(hydroxyethyl)trimethyl ethylenediamine
N-acetyl-o-glucosidinamine	Jeffamine-800	water (control)
creatine	L-thiazolidine-4-carboxylic acid	1-(2-methoxyphenyl) piperazine
1,4,7,10-tetraazacyclododecane tetrahydrochloride	L-thiazolidine-4-carboxylic acid	1-(2-hydroxylethyl) piperazine
HCl water (control)	piperazine	bis(2-aminopropyl)-PEG-1900,
ethylenediamine	alloxan	thiosinamin
3-acetoxy-2(1 <i>H</i>)-pyridone	sulfamide	3-(2-aminoethylamino-propyl)-trimethoxy-silane
isonipecotic acid	Jeffamine-2070	bis(3-aminopropyl)amine
D,L-pipecolinic acid	cycloheximide	triethylenetetramine
		2,3-dihydroxypyridine

SCHEME 2: Schematic Representation of the HT Method Used to Screen for Successful Polymer Phase Transfer Chemistries in Multiwell Plates^a



^a Step 1, the amine library is added to individual multiwell plates at 3-fold redundancy. Step 2, chloroform solutions containing the SPIO nanoparticles and a particular maleic anhydride copolymer are added to the wells. Step 3, water is added to the wells above the chloroform phase. Step 4, the chloroform is removed via heating and ‘hit’ polymer chemistries* are observed when the water solution becomes dark from water dispersed SPIO nanoparticles.

glass ampule. If the reaction did not proceed spontaneously, the chloroform phase was then removed via rotovaporation. SPIO solutions were then cleaned via repeated ultracentrifugation at 30k rpm.

Cryo-Transmission Electron Microscopy (Cryo-TEM). A laboratory-built humidity-controlled vitrification system was used to prepare the nanoparticles for imaging in a thin layer of vitrified ice using cryo-TEM. Humidity was kept close to 80% for all experiments, and ambient temperature was 22 °C. Copper grids (200 mesh) coated with perforated carbon film (Lacey carbon film: ProSciTech, Kirwan, Australia) were used for all experiments. Aliquots (4 μL) of the sample were pipetted onto each grid prior to plunging. After 30 s adsorption time the grid was blotted manually using Whatman 541 filter paper for ~2 s. Blotting time was optimized for each sample. The grid was then plunged into liquid ethane cooled by liquid nitrogen. Frozen grids were stored in liquid nitrogen until required.

The samples were examined using a Gatan 626 cryoholder (Gatan, Pleasanton, CA) and Tecnai 12 transmission electron microscope (FEI, Eindhoven, The Netherlands) at an operating voltage of 120 kV. At all times low-dose procedures were followed, using an electron dose of 8–10 e⁻/Å² for all imaging. Images were recorded using a Megaview III CCD camera and AnalySIS camera control software (Olympus.) using magnifications in the range 60 000–110 000×.

The samples were also imaged by negative stain TEM: in this case carbon-coated 300-mesh copper grids were glow-discharged in nitrogen for 15 s, and a 4–5 μL aliquot of nanoparticle suspension was then allowed to settle on the grid for 1 min. The excess sample was wicked away with filter paper, and a 5 μL water wash was then followed by staining with 2% uranyl acetate (Agar). The grids were examined at room temperature using the microscope described above under standard imaging conditions.

Dynamic Light Scattering Analysis. Particle size measurements were performed using a Zetasizer-Nano instrument (Malvern, UK). Particle sizes were measured in Milli-Q water

using samples appropriately diluted. The analysis was performed at 25 °C and for each sample, the mean diameter of six determinations was calculated.

ICP Analysis. ICP-OES analysis was performed using a Varian-Vista instrument. In preparing solutions for analysis, 20 μL of nanoparticle solution was dissolved in 200 μL of concentrated nitric acid at 70 °C for 2 h. Samples were then transferred quantitatively into a 10 mL standard volumetric flask. Samples were then filtered through 0.22 μm filters before analysis, the average of three separate solutions per nanoparticle batch was taken to determine total iron content of each ‘hit’ phase transferred nanoparticle solution.

MRI Relaxivity Measurements. A HT MRI screening technique was used to evaluate the NMR relaxation properties of the SPIO particle solutions at 3 T using a method similar to that previously reported.³⁶ For MRI relaxivity measurements, 280 μL of Resovist and each ‘hit’ SPIO polymer chemistries were placed in a 96-well plate at five different Fe concentrations serially diluted from 200 to 12.5 μM. The 96-well plate was then imaged at 23 °C in Siemens (Germany) 3 T TRIO MRI scanner using a body transmit radio frequency coil and a 12-channel radiofrequency receiver coil. For quantifying R2 relaxivity a Carr–Purcell Meiboom and Gill multiecho spin echo sequence³⁹ was used to acquire 32 images at echo times (TE) ranging from 11.5 to 310.5 ms with a repetition time (TR) of 3 s. To quantify R2* a FLASH multiecho gradient echo sequence⁴⁰ was used to acquire five different images at TEs ranging from 5.45 to 15.37 ms with a TR of 20 ms and flip angle of 20°. Lastly, to quantify R1 the FLASH sequence was used to acquire seven images using seven different flip angles ranging from 2° to 90° with a TR/TE of 20/5.45 ms. All images were acquired with a 3 mm slice thickness, 100 mm FOV, 192 × 154 matrix size and two averages. Zero filling was used to reconstruct all images to a matrix size of 256 × 256.

To calculate R2 and R2* the signal from regions of interest (>40 voxels) centered within each well was averaged and plotted as a function of TE. The R2 and R2* values were then calculated (as the decay constants) by numerically fitting (using a nonlinear least-squares algorithm (Matlab, Natick, MA)) the data to a monoexponential equation:

$$S = S_0 \exp(-TE \cdot R2) \quad (1)$$

where S_0 is the equilibrium signal when $TE \ll 1/R2$.

A similar approach was used to calculate R1 except the data was plotted as a function of the flip angle and fitted to the signal versus flip angle equation:

$$S = S_0 \sin \theta \frac{1 - \exp(-TR \cdot R1)}{1 - \cos \theta \exp(-TR \cdot R1)} \quad (2)$$

where θ is the excitation flip angle and S_0 is the equilibrium signal when $TR \gg 1/R1$ and θ approaches 1.

The respective relaxivities of each SPIO hit is the linear gradient of the R1, R2, and R2* data plotted as a function of Fe concentration. Therefore, a linear least-squares analysis (Matlab) was used to quantify the R1, R2, and R2* relaxivities.

Results and Discussion

The nanoparticles produced (Figure 1A) in this work were extremely monodisperse, owing to the excellent production method reported by Park et al.²⁰ Figure 1B shows a cryo-TEM image of the nanoparticles in water after phase transfer using a

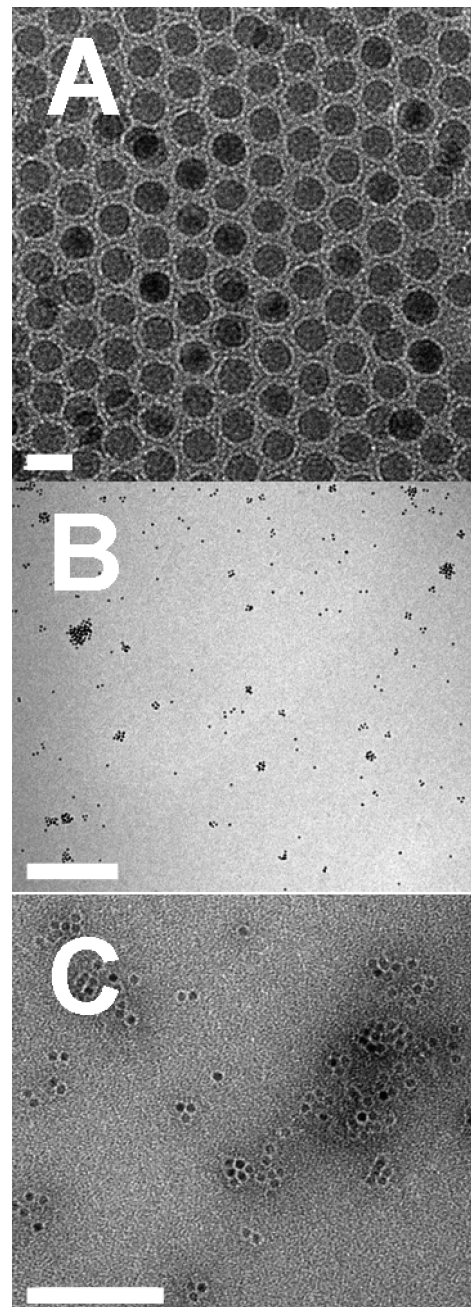


Figure 1. (A) TEM image of the monodisperse hydrophobic 8 nm SPIO nanoparticles produced via the Park method²⁰ (scale bar 10 nm). (B) Cryo-TEM image of dispersed nanoparticles. This typical field of view shows nanoparticles existing as they would in solution, mostly as single particles or small clusters of 2–3 particles, with a small number of larger clusters. (Scale bar 200 nm) Figure 1C; negatively stained nanoparticles showing the polymer coating around the cores (scale bar 100 nm).

bis-amino Jeffamine (M_w 800, CAS no. 65605-36-9), one of the hits in this study. Interestingly, no significant effect of polymer molecular weight and ring-opening chemistry was seen in terms of the mean hydrodynamic radius of the water-soluble SPIO nanoparticles measured via dynamic light scattering (DLS) analysis (intensity and number vs size, see Supporting Information). The average hydrodynamic particle size observed of the 8 nm iron oxide core nanoparticles varied between 22 and 30 nm by number mean. Low-molecular-weight amines such as ethanolamine produced the smallest particle sizes and larger macromolecules such as the Jeffamines resulted in nanoparticles with slightly larger and broader hydrodynamic radii. We believe

this means any change in the stabilizing polymer structure around the SPIO nanoparticle only varies to a small degree or any significant effect is not seen possibly due to the fact the bulk of the scattering will be due to the iron oxide cores themselves and inherent errors in the size measurement⁴¹ due to slight changes in the refractive index of the different polymer chemistries used. It has previously been reported that little change in mean SPIO nanoparticle hydrodynamic radii is observed with significant changes in stabilizing polymer molecular weight.⁴² Evidence of a small amount of larger nanoparticle agglomerates with some of the ring-opening chemistries used is evident from the DLS Intensity vs size data (see Supporting Information). The amines used which did not appear to result in any degree of aggregation observed via DLS analysis were *N,N*-bis(hydroxyethyl)trimethylenediamine, 2-aminoethyl-amino ethanol and *N*-methyl-D-glucamine. From the cryo-TEM image of the phase transferred nanoparticles using Jeffamine, it can be seen that the nanoparticles are fairly monodisperse with minimal agglomerates detected. Some particles exist as 2–3 SPIO cores linked together and a few larger agglomerates are observed. The mean particle size measured via cryo-TEM was 30 ± 13 nm. Cryo-TEM image analysis revealed that 46% of the particles observed were single SPIOs, 23% were twin particles and 31% were agglomerates of three or more particles.

The discrepancy in the particle sizes measured using Jeffamine via DLS analysis (25 nm number mean and 100 nm intensity mean) and cryo-TEM (30 ± 13 nm) is likely due to the small number of larger agglomerates observed. DLS assumes a number of key physical properties when calculating particle size including uniform density (refractive index) of the particle and spherical particle shape. This is obviously not the case when groups of SPIO cores are bound together in solution after phase transferring. A small number of larger multiple SPIO core agglomerates as observed from the cryo-TEM data will skew the mean particle diameter measured via DLS to larger particle sizes. To further the understanding of the size of the polymer coatings around the SPIO cores a negative stain TEM was performed on the material. Imaging the particles by negative stain TEM reveals the polymer coating in a nonhydrated state. The diameter of the stained particles is of the order of 14–15 nm indicating their exists a 2–3 nm dried polymer coating dense enough to be resolved around each iron oxide core. This highlights the fact that the stabilizing polymer shell is quite thin. Evidence to this effect and the factors which influence the size of the stabilizing polymer shell has recently been reported by Sperling et al.⁴¹ In the negative stain TEM analysis the particles show a strong tendency to aggregate. In view of the fact that they are considerably more disperse in the frozen hydrated images, the aggregation seen here is most likely a drying phenomenon.

As mentioned, for the HT screen of potential SPIO water solubilizing compounds, amines were arrayed at 3-fold redundancy and a ‘hit’ chemistry was only investigated if two out of three wells appeared to result in the stable suspension of nanoparticles in PBS after 1 week. From the HT screen performed, 19 possible ‘hit’ ring-opening chemistries were discovered. Figure 2 shows an image of a multiwell plate after a HT screen was performed with a selection of the amines listed in Table 2. It can be seen that a number of wells (circled in red) appear to have SPIO nanoparticles in solution after removal of the chloroform phase and addition of PBS. Some ‘hits’ when scaled up were found to be unsuccessful and no further work was performed to optimize the phase transfer of those compounds. Occasionally the amine used would oxidize upon

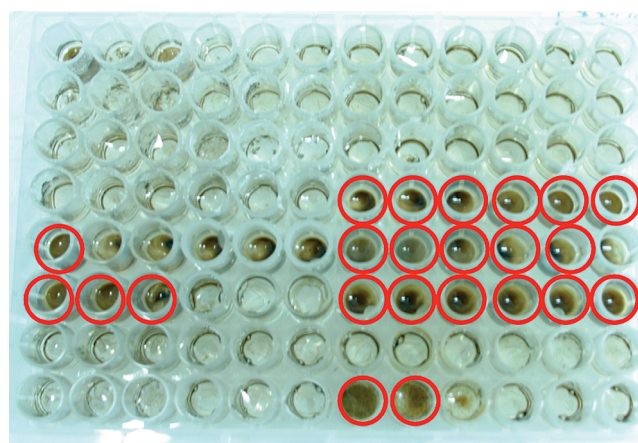


Figure 2. Image of a 96-well plate after a HT phase transfer screen on the poly(octadecene-*co*-maleic anhydride) copolymer ring-opening chemistries listed in Table 1 was performed. Possible ‘hits’ have been circled in red.

TABLE 3: List of ‘Hit’ Amines That Resulted in the Phase Transfer of the SPIO Nanoparticles after Ring-Opening the Adsorbed PMAO, M_n 30–50k

ethanolamine	2-aminoethylamino ethanol
Jeffamines	1-(2-hydroxylethyl) piperazine
<i>N</i> -methyl-D-glucamine	2-(butylamino)ethanol
morpholine	<i>N,N</i> -bis(hydroxyethyl)trimethylenediamine
4-amino-1-butanol	methoxy-PEG-amine
triethylenetetraamine	<i>n</i> -acetyl piperazine
bis(3-aminopropyl)amine	2-(2-aminoethoxy)ethanol

heating and turn brown giving false positives and other compounds appeared to give a ‘stabilizing’ effect to the dissolution of the nanoparticles that was not present once the excess amine and polymer was removed from solution. From the 87-member initial amino library, 14 true ‘hit’ ring-opening chemistries were discovered, indicating that studies with a greater number of anhydride copolymer chemistries and anhydride reactive compounds may result in even further ring-opening chemistries being discovered. The results indicate that this method of phase transfer is not unique to a small number of ring-opening compounds as previously reported.^{23,28,32}

Table 3 and Figure 3 list the ‘hit’ amine ring-opening chemistries discovered in this work. The hits include two polymer chemistries consisting of poly(ethylene glycol) (PEG) and poly(ethylene oxide-*co*-polypropylene oxide), Jeffamine, that are end-functionalized with either one or two primary amines respectively. These would be expected to provide the most effective ‘stealthlike’ properties from macrophage uptake by the reticuloendothelial system (RES) *in vivo*.¹⁷ Ongoing work is being conducted to assess the viability of these candidates *in vitro* and *in vivo* and is beyond the scope of this paper. From the ring-opening chemistries discovered there were some interesting trends and observations noted. The ‘piperidene and piperazine’ family of ‘hit’ ring-opening chemistries, including morpholine, indicates that the secondary amine on the cyclic compound is obviously quite reactive. In previous work we have also noted the success of reactions with this class of secondary amines with maleic anhydride copolymers.²⁴

A number of new bi-, tri-, and tetra-amino ‘hit’ ring-opening compounds were also discovered in the study reported here (Table 3). We believe these compounds are advantageous for some applications as first, the compounds will allow the chemical cross-linking of the stabilizing polymer core around the hydrophobic nanoparticles, and second, residual primary

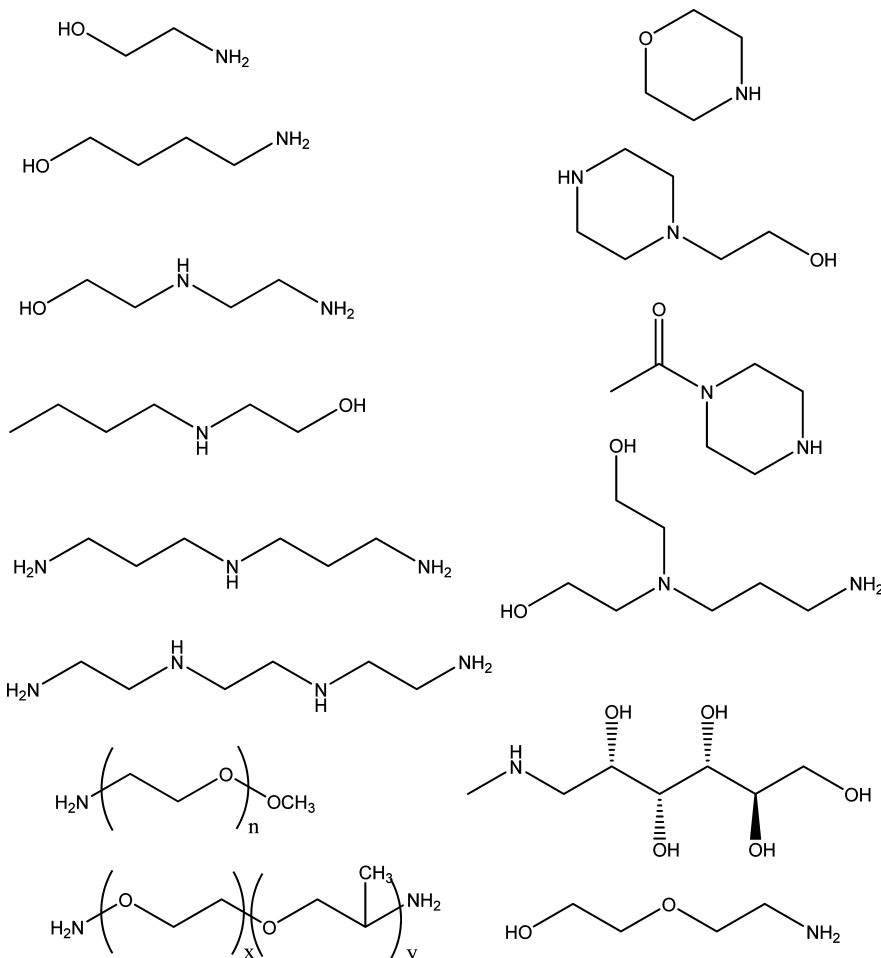


Figure 3. Complete list of the chemical structures (from Table 2) of the ‘hit’ amine functional compounds that resulted in the phase transfer of the SPIO nanoparticles after ring-opening the adsorbed PMAO, M_n 30–50k.

amine groups should be available for further bioconjugation and targeted work. In an excellent paper by Wiessleder et al.⁴³ they reported a combinatorial small molecule study of functionalized magnetofluorescent nanoparticles and investigated the passive targeting of the decorated nanoparticles upon various cell lines in vitro and a tumor model in vivo. We believe the chemistry reported in our work would be extremely amenable to such further studies due to the versatility and efficiency of the anhydride–amine reaction. We have for example seen that we can partially ring open the anhydride polymer to impart water solubility to the SPIO then subsequently react the residual anhydride units on the stabilizing polymer chains with further amines that otherwise would not result in a stabilized nanoparticle system. A number of the hit polymer chemistries shown here are also effective at transferring CdSe quantum dot nanoparticles.³⁵ In a study by Wu et al.,⁴⁴ quantum dots were successfully phase transferred using a modified poly(acrylic acid) polymer modified with octylamine. Anderson et al.⁴⁵ also investigated the use of modified poly(acrylic acid) polymers for the effective phase transfer of nanoparticles using various primary amine containing small chain hydrocarbons. The structures of these polymers are somewhat similar to the ring-opening chemistries used in our work.

During the scale up of the ‘hit’ amine compounds it was noted that some of the ‘hits’ were extremely efficient at phase transferring all of the SPIOs from the chloroform phase under ambient conditions over a few hours. In particular, *N,N*-bis(hydroxyethyl)trimethylenediamine, *N*-methyl-D-glucamine

and bis(3-aminopropyl)amine were particularly effective. These three compounds were subsequently chosen to be reacted with four synthesized maleic anhydride copolymers to investigate any possible molecular weight and copolymer chemistry effects in the stabilization of the nanoparticles. All of the polymers which were made via the RAFT process resulted in different measures of success in terms of the control observed in the polymers polydispersity index (PD) as reported in the Experimental Methods section (Table 1). The results of this study can be seen in Figure 4 where vials containing the SPIOs, polymer, and amine in chloroform have had water added above them. The vials were allowed to react under ambient conditions overnight then an image of the vials showing the efficiency of the phase transfer was taken.

From the results in Figure 4, the effect of molecular weight with different copolymer chemistries on the stabilization of the nanoparticles is evident when comparing the poly(octadecene-*co*-maleic anhydride) copolymer, P1 and P5, of molecular weights 6.4k and 30–50k, respectively. It can be seen that the higher molecular weight polymer, P5, efficiently phase transfers the nanoparticles with all three different amines used while the P1 polymer is extremely poor. When using the P1 polymer for the amines, *N,N*-bis(hydroxyethyl)trimethylenediamine and *N*-methyl-D-glucamine the phase transfer was extremely inefficient with most nanoparticles either being located at the water–chloroform interface or remaining in chloroform. The phase transfer of the SPIOs by the maleic anhydride copolymers will arise from a combination of both steric and charge stabilization

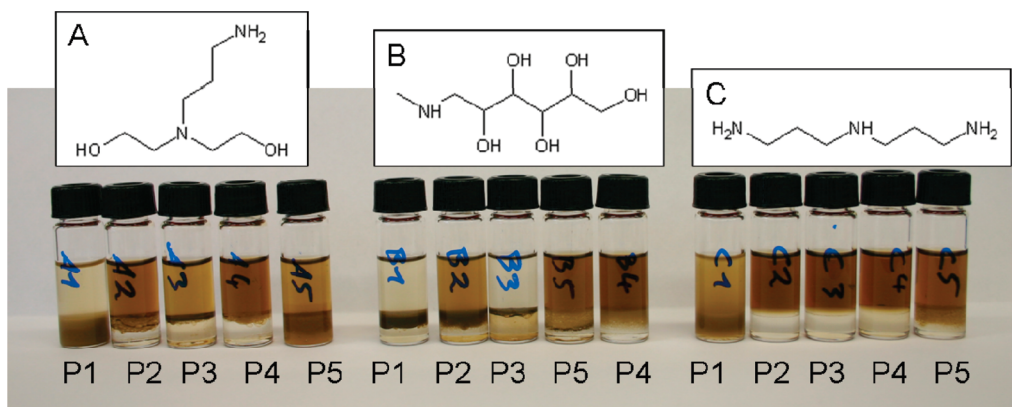


Figure 4. Results of the attempted phase transfer of SPIO nanoparticles coated with five different polymers (P1–P5) and reacted with three different amines from left to right in the image (A, B, C). The chloroform phase is in the bottom of the vials and the water phase is above. An efficient phase transfer is indicated by a dark brown aqueous solution with little aggregation at the solvent interface or residual particles in the chloroform phase; Polymer IDs; P1, poly(octadecene-*co*-maleic anhydride) PD = 1.53, M_n = 6500; P2, poly(styrene-*co*-maleic anhydride) PD = 1.16, M_n = 2000; P3, poly(styrene-*co*-maleic anhydride) PD = 1.3, M_n = 6400; P4, poly(*n*-butyl vinyl ether-*co*-maleic anhydride) PD = 2.31, M_n = 4900; P5, commercial poly(octadecene-*co*-maleic anhydride) CAS no. 25266-02-8, PD = not supplied, M_n = 30–50k; Amine IDs; A, *N,N*-bis(hydroxyethyl)trimethylenediamine; B, *N*-methyl-D-glucamine; C, bis-(3-aminopropyl)amine.

effects. Therefore, the lower-molecular-weight polymer has not suitably fulfilled the solubility conditions required at this lower molecular weight. Obviously for long-term stability in buffer, it would be expected that a significant steric component must be present as the repellent surface charge on these particles will be sufficiently screened in 0.1 M PBS.

The poly(styrene-*co*-maleic anhydride) RAFT polymers P2 and P3 with molecular weights of 2000 and 6400, respectively, display an opposite effect in terms of phase transfer efficiency with copolymer molecular weight. We believe this is due to the decreasing water solubility of the styrene copolymer system observed with increasing molecular weight. The effect of decreasing polymer solubility with increasing molecular weight is well documented.^{46,47} Other factors affecting the observed discrepancy in the two polymers SPIO phase transfer efficiency may also include the polymer chain chemistry, composition, stereochemistry, and reactivity of the anhydride units.⁴⁶ The poly(*n*-butyl vinyl ether-*co*-maleic anhydride) polymer was successful at phase transferring with each of the three amine ring-opening chemistries tested. These results show that the phase transfer of hydrophobic inorganic metal nanoparticles is not limited to maleic anhydride copolymers with long hydrocarbon comonomers. Even bulky side groups such as styrene are capable of successfully binding with the hydrocarbon chains emanating from the SPIO core surfaces either through interdigitation or hydrophobic–hydrophobic interactions.

Stability testing of all the nanoparticles in Figure 4 was performed in PBS for 1 month. It was found that the only particles to remain stable in buffer after this time with all three amines used were those transferred using the commercial poly(octadecene-*co*-maleic anhydride) polymer. We believe this is due primarily to a molecular weight effect as discussed, whereby the higher M_w polymer (M_n = 30–50k) allows for significant charge and steric stabilization of the SPIO nanoparticles while the lower molecular weight polymer does not. Interestingly, the poly(*n*-butyl vinyl ether-*co*-maleic anhydride) polymer when reacted with *N*-methyl-D-glucamine was also stable after one month in buffer. None of the poly(styrene-*co*-maleic anhydride) transferred polymers were stable in buffer for more than 48 h. The poly(styrene-*co*-maleic anhydride) polymer backbone would be expected to have less conformational freedom than the butyl vinyl ether and octadecene copolymer structures which would further reduce the buffer

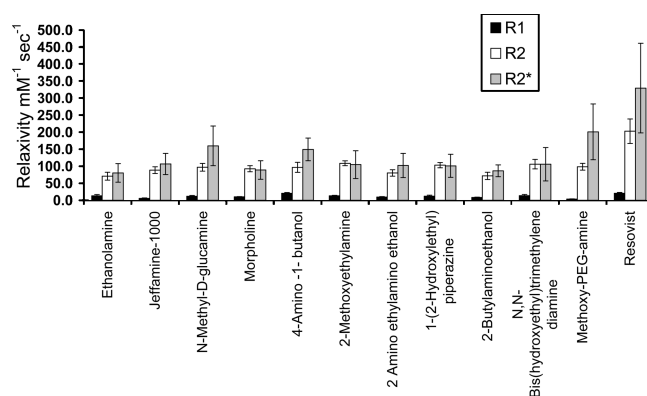


Figure 5. Relaxivities (R1, R2, R2*) measured in a HT MRI screen of the SPIO nanoparticles stabilized with the 'hit' poly(octadecene-*co*-maleic anhydride)copolymer ring-opening chemistries. Resovist data is shown as a comparison. 95% confidence intervals are reported.

stability of SPIOs produced using this more conformationally restricted polymer. It should be noted here that Resovist, a clinically used SPIO formulation stabilized with dextran precipitated from buffer solution over a period of 4 days.

The magnetic properties of the 'hit' amine chemistries using the commercially available poly(octadecene-*co*-maleic anhydride) copolymer were screened in multiwell plates inside a magnetic resonance imaging machine and the corresponding, R1, R2, and R2* relaxivities were calculated. The results of which can be seen in Figure 5 along with the measurements of Resovist, a clinically used SPIO formulation stabilized by a dextran polymer. The HT MRI screening of the individual properties of each SPIO 'hit' in this manner dramatically improves the speed and efficiency by which these measurements can be made. Traditionally, relaxivity measurements are performed in a low-field NMR and are time-consuming. By arraying the SPIO formulations into multiwell plates, the magnetic properties of hundreds of nanoparticles can be screened in a matter of minutes at a clinically relevant magnetic field compared to weeks using a low-field NMR instrument. In the only other HT MRI study we are aware of, Hogemann et al.³⁶ evaluated the binding of a library of peptide–nanoparticle conjugates against cell lines in multiwell plates using MR imaging.

The measured relaxivity data in Figure 5 show that within the error of the measurements the R2 relaxivities of each SPIO

used in this work is fairly similar. This would be expected as the transverse relaxation T2 is primarily affected by the inherent magnetic properties of the nanoparticle itself.²¹ The transverse relaxation of SPIO nanoparticles has shown to be affected somewhat by stabilizing ligand surface chemistries⁴⁸ and their may be some effects of this nature in our work with the amines N-methyl-D-glucamine, 4-amino-1-butanol, and methoxy-PEG-amine. In recent work by Tromsdorf et al.⁴⁸ it was shown that the R2* of a MnFe₂O₄ nanocrystal can vary quite dramatically depending on the size of the nanocrystal and stabilizing material due to differences in nanocrystal aggregation. Interestingly there are some statistically significant changes observed in the R1 relaxivity of each particle ring-opened and phase-transferred with different nucleophiles. As the longitudinal relaxation rate T1 is primarily affected by inner sphere water, it seems this measurement may be picking up the subtle changes of polymer chemistry on each 'hit' SPIO coating. The relaxivities measured of Resovist are significantly greater than that of the SPIOs used in this work. This is due to the fact that Resovist is a composite SPIO consisting of agglomerations of ultrasmall SPIO nanoparticles of 4 nm diameter surrounded in a dextran matrix to a final mean hydrodynamic size of ~65 nm. The R1/R2 relaxivities of Resovist measured experimentally ($20 \pm 3/203 \pm 36$ mM⁻¹ s⁻¹) consistent with those ($4.6 \pm 0.3/143 \pm 12$ mM⁻¹ s⁻¹) previously reported,⁴⁹ given our experiments were conducted at 23 °C and not 37 °C.

Conclusions

In this work we have demonstrated the usefulness of HT screening and characterization methods in the field of inorganic metal nanoparticle phase transfer. We believe the techniques described here have applicability for use, not just in medical imaging contrast agent development but in nanomaterials research generally. The use of a HT MRI technique in conjunction with a combinatorial multiwell chemical screening process has proven invaluable in discovering novel amphiphilic phase transfer polymer chemistries based on maleic anhydride copolymers. We have found that copolymer chemistry (hydrophobic groups), the choice of primary or secondary amine molecule used to ring open the anhydride and polymer molecular weight play a critical role. The use of HT techniques has proven invaluable in determining suitable polymer chemistries that provide sufficient stabilization for long-term stability in buffer of hydrophobic inorganic metal nanoparticles.

Acknowledgment. Paul Mulvaney acknowledges the support of DEST through Grant CG110036.

Supporting Information Available: DLS data (intensity and number vs size) of the 'hit' amines that resulted in the phase transfer of SPIO nanoparticles after ring-opening with a poly-(octadecene-*co*-maleic anhydride) polymer. This material is available free of charge via the Internet at <http://pubs.acs.org>.

References and Notes

- (1) Forster, S.; Antonietti, M. Amphiphilic block copolymers in structure-controlled nanomaterial hybrids. *Adv. Mater.* **1998**, *10* (3), 195+.
- (2) Shipway, A. N.; Katz, E.; Willner, I. Nanoparticle arrays on surfaces for electronic, optical, and sensor applications. *Chemphyschem* **2000**, *1* (1), 18–52.
- (3) Medintz, I. L.; Uyeda, H. T.; Goldman, E. R.; Mattoussi, H. Quantum dot bioconjugates for imaging, labelling and sensing. *Nat. Mater.* **2005**, *4* (6), 435–446.
- (4) Michalet, X.; Pinaud, F. F.; Bentolila, L. A.; Tsay, J. M.; Doose, S.; Li, J. J.; Sundaresan, G.; Wu, A. M.; Gambhir, S. S.; Weiss, S. Quantum dots for live cells, in vivo imaging, and diagnostics. *Science* **2005**, *307* (5709), 538–544.
- (5) Corot, C.; Robert, P.; Idee, J. M.; Port, M. Recent advances in iron oxide nanocrystal technology for medical imaging. *Adv. Drug Delivery Rev.* **2006**, *58* (14), 1471–1504.
- (6) Reimer, P.; Tombach, B.; Daldrup, H.; Hesse, T.; Sander, G.; Balzer, T.; Shamsi, K.; Berns, T.; Rummeny, E. J.; Peters, P. E. New MR contrast agents in the diagnosis of liver lesions. Preliminary clinical experience with the hepatic biliary Eovist (gadolinium-EOB-DTPA) and the RES-specific Resovist (SH U 555 A). *Der Radiologe* **1996**, *36* (2), 124–133.
- (7) Gao, S.; Shi, Y.; Zhang, S.; Jiang, K.; Yang, S.; Li, Z.; Takayama-Muromachi, E. Biopolymer-Assisted Green Synthesis of Iron Oxide Nanoparticles and Their Magnetic Properties. *J. Phys. Chem. C* **2008**, *112* (28), 10398–10401.
- (8) Huang, J. H.; Parab, H. J.; Lai, T. C.; Hsiao, M.; Chen, C. H.; Sheu, H. S.; Chen, J. M.; Tsai, D. P.; Hwu, Y. K.; Liu, R. S. Investigation of the Growth Mechanism of Iron Oxide Nanoparticles via a Seed-Mediated Method and Its Cytotoxicity Studies. *J. Phys. Chem. C* **2008**, *112* (40), 15684–15690.
- (9) Rovers, S. A.; Hoogenboom, R.; Kemmere, M. F.; Keurentjes, J. T. F. Relaxation Processes of Superparamagnetic Iron Oxide Nanoparticles in Liquid and Incorporated in Poly(methyl methacrylate). *J. Phys. Chem. C* **2008**, *112* (40), 15643–15646.
- (10) Shtykova, E. V.; Huang, X.; Remmes, N.; Baxter, D.; Stein, B.; Dragnea, B.; Svergun, D. I.; Bronstein, L. M. Structure and Properties of Iron Oxide Nanoparticles Encapsulated with Phospholipids with Poly(ethylene glycol) Tails. *J. Phys. Chem. C* **2007**, *111* (49), 18078–18086.
- (11) Zhu, A.; Yuan, L.; Dai, S. Preparation of Well-Dispersed Superparamagnetic Iron Oxide Nanoparticles in Aqueous Solution with Biocompatible N-Succinyl-O-carboxymethylchitosan. *J. Phys. Chem. C* **2008**, *112* (14), 5432–5438.
- (12) Berry, C. C.; Curtis, A. S. G. Functionalisation of magnetic nanoparticles for applications in biomedicine. *J. Phys. D-Appl. Phys.* **2003**, *36* (13), R198–R206.
- (13) Duguet, E.; Vasseur, S.; Mornet, S.; Devoisselle, J. M. Magnetic nanoparticles and their applications in medicine. *Nanomedicine* **2006**, *1* (2), 157–168.
- (14) Laurent, S.; Forge, D.; Port, M.; Roch, A.; Robic, C.; Elst, L. V.; Muller, R. N. Magnetic iron oxide nanoparticles: Synthesis, stabilization, vectorization, physicochemical characterizations, and biological applications. *Chem. Rev.* **2008**, *108* (6), 2064–2110.
- (15) McCarthy, J. R.; Kelly, K. A.; Sun, E. Y.; Weissleder, R. Targeted delivery of multifunctional magnetic nanoparticles. *Nanomedicine* **2007**, *2* (2), 153–167.
- (16) Tartaj, P.; Morales, M. D.; Veintemillas-Verdaguer, S.; Gonzalez-Carreno, T.; Serna, C. J. The preparation of magnetic nanoparticles for applications in biomedicine. *J. Phys. D-Appl. Phys.* **2003**, *36* (13), R182–R197.
- (17) Gupta, A. K.; Gupta, M. Synthesis and surface engineering of iron oxide nanoparticles for biomedical applications. *Biomaterials* **2005**, *26* (18), 3995–4021.
- (18) Cao, S. W.; Zhu, Y. J.; Ma, M. Y.; Li, L.; Zhang, L. Hierarchically nanostructured magnetic hollow spheres of Fe₃O₄ and γ-Fe₂O₃: Preparation and potential application in drug delivery. *J. Phys. Chem. C* **2008**, *112* (6), 1851–1856.
- (19) Chertok, B.; Moffat, B. A.; David, A. E.; Yu, F. Q.; Bergemann, C.; Ross, B. D.; Yang, V. C. Iron oxide nanoparticles as a drug delivery vehicle for MRI monitored magnetic targeting of brain tumors. *Biomaterials* **2008**, *29* (4), 487–496.
- (20) Park, J.; An, K. J.; Hwang, Y. S.; Park, J. G.; Noh, H. J.; Kim, J. Y.; Park, J. H.; Hwang, N. M.; Hyeon, T. Ultra-large-scale syntheses of monodisperse nanocrystals. *Nat. Mater.* **2004**, *3* (12), 891–895.
- (21) Jun, Y. W.; Lee, J. H.; Cheon, J. Chemical design of nanoparticle probes for high-performance magnetic resonance imaging. *Angew. Chem., Int. Ed.* **2008**, *47* (28), 5122–5135.
- (22) Amstad, E.; Zurcher, S.; Mashaghi, A.; Wong, J. Y.; Textor, M.; Reimhult, E. Surface Functionalization of Single Superparamagnetic Iron Oxide Nanoparticles for Targeted Magnetic Resonance Imaging. *Small* **2009**, *5* (11), 1334–1342.
- (23) Pellegrino, T.; Manna, L.; Kudera, S.; Liedl, T.; Koktysh, D.; Rogach, A. L.; Keller, S.; Radler, J.; Natile, G.; Parak, W. J. Hydrophobic nanocrystals coated with an amphiphilic polymer shell: A general route to water soluble nanocrystals. *Nano Lett.* **2004**, *4* (4), 703–707.
- (24) Muir, B. W.; Barden, M. C.; Collett, S. P.; Gorse, A. D.; Monteiro, R.; Yang, L.; McDougall, N. A.; Gould, S.; Maeji, N. J. High-throughput optimization of surfaces for antibody immobilization using metal complexes. *Anal. Biochem.* **2007**, *363* (1), 97–107.
- (25) Lin, C. A. J.; Sperling, R. A.; Li, J. K.; Yang, T. Y.; Li, P. Y.; Zanella, M.; Chang, W. H.; Parak, W. G. J. Design of an amphiphilic polymer for nanoparticle coating and functionalization. *Small* **2008**, *4* (3), 334–341.

- (26) Yu, W. W.; Chang, E.; Sayes, C. M.; Drezek, R.; Colvin, V. L. Aqueous dispersion of monodisperse magnetic iron oxide nanocrystals through phase transfer. *Nanotechnology* **2006**, *17* (17), 4483–4487.
- (27) Arbos, P.; Wirth, M.; Arangoa, M. A.; Gabor, F.; Irache, J. M. Gantrez (R) AN as a new polymer for the preparation of ligand-nanoparticle conjugates. *J. Controlled Release* **2002**, *83* (3), 321–330.
- (28) Di Corato, R.; Quarta, A.; Piacenza, P.; Ragusa, A.; Figuerola, A.; Buonsanti, R.; Cingolani, R.; Manna, L.; Pellegrino, T. Water solubilization of hydrophobic nanocrystals by means of poly(maleic anhydride-*alt*-1-octadecene). *J. Mater. Chem.* **2008**, *18* (17), 1991–1996.
- (29) Klumperman, B. Styrene/Maleic Anhydride Macro-RAFT-Mediated Encapsulation. *Macromol. Chem. Phys.* **2006**, *207* (10), 861–863.
- (30) Kobayashi, H.; Sato, N.; Kawamoto, S.; Saga, T.; Hiraga, A.; Ishimori, T.; Konishi, J.; Togashi, K.; Brechbiel, M. W. 3D MR angiography of intratumoral vasculature using a novel macromolecular MR contrast agent. *Magn. Reson. Med.* **2001**, *46* (3), 579–585.
- (31) Yang, J.; Dave, S. R.; Gao, X. H. Quantum dot nanoparcodes: Epitaxial assembly of nanoparticle-polymer complexes in homogeneous solution. *J. Am. Chem. Soc.* **2008**, *130* (15), 5286–5292.
- (32) Yoncheva, K.; Lizarraga, E.; Irache, J. M. Pegylated nanoparticles based on poly(methyl vinyl ether-*co*-maleic anhydride): preparation and evaluation of their bioadhesive properties. *Eur. J. Pharm. Sci.* **2005**, *24* (5), 411–419.
- (33) Yu, W. W.; Chang, E.; Falkner, J. C.; Zhang, J. Y.; Al-Somali, A. M.; Sayes, C. M.; Johns, J.; Drezek, R.; Colvin, V. L. Forming biocompatible and nonaggregated nanocrystals in water using amphiphilic polymers. *J. Am. Chem. Soc.* **2007**, *129* (10), 2871–2879.
- (34) Benderbous, S.; Corot, C.; Jacobs, P.; Bonnemain, B. Superparamagnetic agents: Physicochemical characteristics and preclinical imaging evaluation. *Acad. Radiol.* **1996**, *3*, S292–S294.
- (35) Lees, E. E.; Nguyen, T.-L.; Clayton, A. H. A.; Muir, B. W.; Mulvaney, P., The Preparation of Colloidally Stable, Water-Soluble, Biocompatible, Semiconductor Nanocrystals with a Small Hydrodynamic Diameter. *ACS Nano* 2009.
- (36) Hogemann, D.; Ntziachristos, V.; Josephson, L.; Weissleder, R. High throughput magnetic resonance imaging for evaluating targeted nanoparticle probes. *Bioconjugate Chem.* **2002**, *13* (1), 116–121.
- (37) Chong, Y. K.; Moad, G.; Rizzardo, E.; Thang, S. H. Thiocarbonylthio end group removal from RAFT-synthesized polymers by radical-induced reduction. *Macromolecules* **2007**, *40* (13), 4446–4455.
- (38) Moad, G.; Chiefari, J.; Chong, Y. K.; Krstina, J.; Mayadunne, R. T. A.; Postma, A.; Rizzardo, E.; Thang, S. H. Living free radical polymerization with reversible addition-fragmentation chain transfer (the life of RAFT). *Polym. Int.* **2000**, *49* (9), 993–1001.
- (39) Meiboom, S.; Gill, D. Modified spin echo method for measuring nuclear relaxation times. *Rev. Sci. Instrum.* **1958**, *29*.
- (40) Haase, A.; Snapshot FLASH, M. R. I. Applications to T1, T2, and chemical-shift imaging. *Magn. Reson. Med.* **1990**, *13* (1), 77–89.
- (41) Sperling, R. A.; Liedl, T.; Duhr, S.; Kudera, S.; Zanella, M.; Lin, C. A. J.; Chang, W. H.; Braun, D.; Parak, W. J. Size determination of (Bio)conjugated water-soluble colloidal nanoparticles: A comparison of different techniques. *J. Phys. Chem. C* **2007**, *111* (31), 11552–11559.
- (42) Reddy, G. R.; Bhojani, M. S.; McConville, P.; Moody, J.; Moffat, B. A.; Hall, D. E.; Kim, G.; Koo, Y. E. L.; Woolliscroft, M. J.; Sugai, J. V.; Johnson, T. D.; Philbert, M. A.; Kopelman, R.; Rehemtulla, A.; Ross, B. D. Vascular targeted nanoparticles for imaging and treatment of brain tumors. *Clin. Cancer Res.* **2006**, *12* (22), 6677–6686.
- (43) Weissleder, R.; Kelly, K.; Sun, E. Y.; Shtatland, T.; Josephson, L. Cell-specific targeting of nanoparticles by multivalent attachment of small molecules. *Nat. Biotechnol.* **2005**, *23* (11), 1418–1423.
- (44) Wu, X. Y.; Liu, H. J.; Liu, J. Q.; Haley, K. N.; Treadway, J. A.; Larson, J. P.; Ge, N. F.; Peale, F.; Bruchez, M. P. Immunofluorescent labeling of cancer marker Her2 and other cellular targets with semiconductor quantum dots. *Nat. Biotechnol.* **2003**, *21* (1), 41–46.
- (45) Anderson, R. E.; Chan, W. C. W. Systematic investigation of preparing biocompatible, single, and small ZnS-capped CdSe quantum dots with amphiphilic polymers. *Acs Nano* **2008**, *2* (7), 1341–1352.
- (46) Miller-Chou, B. A.; Koenig, J. L. A review of polymer dissolution. *Prog. Polym. Sci.* **2003**, *28* (8), 1223–1270.
- (47) Ueberreiter, K.; Asmussen, F. Velocity of Dissolution of Polymers 0.1. *J. Polym. Sci.* **1962**, *57* (165), 187–&.
- (48) Tromsdorf, U. I.; Bigall, N. C.; Kaul, M. G.; Bruns, O. T.; Nikolic, M. S.; Mollwitz, B.; Sperling, R. A.; Reimer, R.; Hohenberg, H.; Parak, W. J.; Forster, S.; Beisiegel, U.; Adam, G.; Weller, H. Size and surface effects on the MRI relaxivity of manganese ferrite nanoparticle contrast agents. *Nano Lett.* **2007**, *7* (8), 2422–2427.
- (49) Rohrer, M.; Bauer, H.; Mintorovitch, J.; Requardt, M.; Weinmann, H. J. Comparison of magnetic properties of MRI contrast media solutions at different magnetic field strengths. *Invest. Radiol.* **2005**, *40* (11), 715–24.

JP904846E